CMS Physics Analysis Summary

Contact: cms-pag-conveners-susy@cern.ch 2015/12/15

Inclusive search for supersymmetry using the razor variables at $\sqrt{s} = 13$ TeV

The CMS Collaboration

Abstract

An inclusive search for supersymmetry with the razor variables is performed using a data sample of proton-proton collisions corresponding to an integrated luminosity of 2.1 fb^{-1} collected with the CMS experiment at a center-of-mass energy of $\sqrt{s} =$ 13 TeV. The search covers events with zero or one lepton, and four or more jets in the final state. No significant excess over the background prediction is observed in data, and 95% confidence level exclusion limits are placed on the masses of new heavy particles in a variety of simplified models. Assuming the neutralino is the lightest supersymmetric particle with a mass of 100 GeV and the gluino decays to a neutralino and a bottom quark-antiquark pair, the pair production of gluinos is excluded for gluino masses up to 1650 GeV. For the corresponding decays to top quarks and first or second generation quarks, gluinos with masses up to 1600 GeV and 1350 GeV are excluded, respectively.

1 Introduction

We present a search for physics beyond the Standard Model (SM) using the razor variables [1, 2]. The use of razor variables to search for supersymmetry (SUSY) was established during the LHC Run I by several studies, both by the CMS [2–5] and ATLAS [6, 7] collaborations. The inclusive razor search, based on the combination of final states with and without leptons, has provided a set of competitive and robust limits on squark and gluino masses in various R-parity conserving SUSY scenarios.

We present an inclusive razor search using the LHC 2015 dataset accumulated by the CMS experiment at a center-of-mass energy $\sqrt{s} = 13\,\text{TeV}$ with an integrated luminosity of $2.1\,\text{fb}^{-1}$, targeting the pair production of heavy gluinos. To probe a broad range of signal models in a variety of final states, we perform the search in multiple event categories, based on the presence of specific reconstructed physics objects, such as electrons, muons, and b-jets. With this strategy the purity of specific classes of signals is enhanced in specific event categories while the SM backgrounds are generally suppressed.

In section 2 we describe the razor variables. In section 3, the details of the object identification and event selection requirements are presented, as well as the SUSY signal Monte Carlo samples used in the interpretation of the results. The background, estimated in each event category using a two-dimensional maximum likelihood fit to the distribution of the data in the razor variables is discussed in section 4. In section 5 the systematic uncertainties on the signal are discused, and in section 6 we present the search results. We find that the observed data is compatible with the background-only hypothesis, and set exclusion limits on specific signal models described in section 3.

2 Razor variables

In each event category, described in the following sections, we perform a clustering of the selected leptons and jets in the event into two distinct hemispheres, called megajets. The megajet four-momenta are defined as the sum of the four-momenta of the physics objects in each group. All the possible definitions of the two groups are considered. The definition that minimizes the sum of the invariant masses of the two megajets is selected. The procedure is identical to the one used in past razor searches [5]. The razor variable M_R is computed as:

$$M_R \equiv \sqrt{(P_{\text{j}_1} + P_{\text{j}_2})^2 - (p_z^{\text{j}_1} + p_z^{\text{j}_2})^2}\,, \tag{1}$$

where P_{j_i} ($p_z^{\text{j}_i}$) is the absolute value (the longitudinal value) of the i$^{\text{th}}$-megajet momentum. We also define the transverse variable:

$$M_T^R \equiv \sqrt{\frac{E_T^{miss}(p_T^{j1} + p_T^{j2}) - \vec{p}_T^{\,miss}\cdot(\vec{p}_T^{\,j1} + \vec{p}_T^{\,j2})}{2}}\,, \tag{2}$$

where the missing transverse momentum vector $\vec{p}_T^{\,miss}$ is defined as the projection of the negative vector sum of the momenta of all reconstructed particles in an event on the plane perpendicular to the beam axis, and its magnitude is referred to as E_T^{miss}. The dimensionless variable R^2 is defined as:

$$R^2 \equiv \left(\frac{M_T^R}{M_R}\right)^2. \tag{3}$$

For a typical SUSY decay of a superpartner $\tilde{q}$ decaying into an invisible neutralino $\tilde{\chi}^0$ and the standard model partner q, the mass variable M_R peaks at a characteristic scale $(M_{\tilde{q}}^2 - M_{\tilde{\chi}}^2)/M_{\tilde{q}}$ [1]. For Standard Model background processes, the distribution of M_R has an exponentially decaying shape. The variable R^2 is related to the missing transverse energy and is used to suppress QCD background.

3 Data sample and event selection

Physics objects are defined using the particle-flow (PF) algorithm [8, 9]. The particle-flow algorithm reconstructs and identifies each individual particle with an optimized combination of information from the various elements of the CMS detector. The energy of photons is directly obtained from the ECAL measurement, corrected for zero-suppression effects. The energy of electrons is determined from a combination of the electron momentum at the primary interaction vertex as determined by the tracker, the energy of the corresponding ECAL cluster, and the energy sum of all bremsstrahlung photons spatially compatible with originating from the electron track. The momentum of muons is obtained from the curvature of the corresponding track. The energy of charged hadrons is determined from a combination of their momentum measured in the tracker and the matching ECAL and HCAL energy deposits, corrected for zero-suppression effects and for the response function of the calorimeters to hadronic showers. Finally, the energy of neutral hadrons is obtained from the corresponding corrected ECAL and HCAL energy.

All reconstructed PF candidates are clustered into jets using the anti-k_t algorithm [10, 11] with a size parameter of 0.4. The jet momentum is determined as the vectorial sum of all particle momenta in the jet, and is found from simulation to be within 5% to 10% of the true momentum over the whole p_T spectrum and detector acceptance. An offset correction is applied to jet energies to take into account the contribution from additional proton-proton interactions within the same bunch crossing. Jet energy corrections are derived from simulation, and are confirmed with in-situ measurements of the energy balance in dijet and photon+jet events. Additional selection criteria are applied to each jet to remove spurious jet-like features originating from isolated noise patterns in certain HCAL regions.

Data for this analysis are collected using a suite of dedicated hadronic triggers ("razor triggers"). The razor triggers require selected events to have either two particle-flow jets with $p_T > 80\,\text{GeV}$ or four jets with $p_T > 40\,\text{GeV}$. They also require events to pass cuts on the razor variables $M_R > 200\,\text{GeV}$ and $R^2 > 0.09$, and on the product $(M_R + 300\,\text{GeV}) \times (R^2 + 0.25) > 240\,\text{GeV}$. For the event categories that contain an electron or a muon, the data are collected using the inclusive single-electron and single-muon triggers respectively. These triggers place no requirements on the values of M_R or R^2, and require the presence of at least one isolated muon (electron) with $p_T > 20$ ($p_T > 23$) GeV. For muons (electrons) with $p_T > 50$ ($p_T > 105$) GeV, isolation is not required in the trigger.

Electrons are reconstructed by associating a cluster of energy deposited in the ECAL with a reconstructed track, and must lie in the pseudorapidity range $|\eta| < 2.5$. Two levels of electron selection are used, a tight selection used to isolate signal events containing one lepton and a

veto selection used to improve the signal purity of the zero lepton event sample. The tight electron selection is based on simple rectangular cuts on a set of variables related to the electromagnetic shower shape, the geometric matching of the track to the calorimeter cluster, the track quality and impact parameter, and isolation. The veto electron selection is based on a boosted decision tree that has been trained on a sample including electrons with p_T as low as 5 GeV, and therefore yields more optimal signal to background discrimination. Veto electrons are required to have $p_T > 5$ GeV. For electrons with p_T below 20 GeV, the absolute isolation, calculated by summing the p_T of all particle flow candidates within a ΔR cone of 0.3, is required to be less than 5 GeV. For electrons with $p_T > 20$ GeV, we use the mini-isolation variable whose cone size ΔR is defined as:

$$\Delta R = \begin{cases} 0.2, & p_T \leq 50 \text{ GeV} \\ \frac{10\text{GeV}}{p_T}, & 50 \text{ GeV} \leq p_T \leq 200 \text{ GeV} \\ 0.05, & p_T \geq 200 \text{ GeV} \end{cases} \quad (4)$$

The cone of the mini-isolation shrinks as the p_T of the electron increases, which improves the efficiency for electrons decaying from boosted top quarks and in general for electrons in events with many jets. For the tight electron selection, we require that the mini-isolation divided by the p_T of the electron is less than 0.1, while for the veto selection we require it to be less than 0.2. The isolation variables are corrected for pileup contributions through an estimate of the average energy density measured in the event. The selection efficiency is about 80% for tight electrons and about 90% for veto electrons.

Similar to electrons, there are two levels of muon selection, a tight muon selection and a veto muon selection. All selected muons are required to have $p_T > 5$ GeV, and lie in the pseudorapidity range $|\eta| < 2.4$. We use a cut-based muon selection where the selection utilizes the quality of the track fit, the number of detector hits used in the tracking algorithm, and the compatibility between track segments. The veto selection uses a looser set of requirements on these variables than the tight selection. The impact parameter in the $\rho - \phi$ plane is required to be less than 0.2 cm, and the absolute value of the 3D impact parameter significance must be less than 4. Muons with p_T below 20 GeV are required to have absolute isolation less than 10 GeV, while muons with $p_T > 20$ GeV are required to have the mini-isolation divided by the p_T of the muon to be less than 0.2. The isolation is pileup corrected in the same way as described above for electrons. The selection efficiency is about 80% for tight muons, and about 95% for veto muons.

To identify jets that originate from b-hadron decays, we use the combined secondary vertex (CSV) b-jet tagger, which uses the inclusive vertex finder to select b-jets [12]. The medium working point, requiring the discriminator to be larger than 0.890, is used to define the event categories for the search signal regions. The probability of identifying b quarks as b-jets is approximately 70% for a sample of $t\bar{t}$ events, while the probability of misidentifying light-quarks or gluons as b-jets is about 1.5%.

3.1 Baseline event selection

The strategy for this analysis is to separate events into different categories based on the presence of certain physics objects. For each event category, we compute the razor variables M_R and R^2, and search for resonances or anomalous excesses in the tails of the M_R and R^2 distributions. The standard model background exhibits an exponentially decaying distribution in the two razor variables, while a typical SUSY signal exhibits a broad peak in M_R and a long tail in R^2.

To maximize sensitivity to various possible types of signal processes, we perform the search in leptonic and hadronic final states. Events that fall into the categories with an identified charged lepton provide an additional sensitivity to signals that contain a W or Z boson in the decay chain. Event categories are defined exclusively in the following sequential order:

- Muon Multijet: All events containing at least one muon and four or more selected jets.
- Electron Multijet: All other events containing at least one electron and four or more selected jets.
- Multijet: All other events containing at least four or more selected jets.

Events with two or more tight electrons or muons are rejected.

The main selection criteria in this analysis are driven by the trigger requirements, such as M_R and R^2 thresholds in the hadronic triggers, and lepton p_T in the leptonic ones. For the Multijet event category, where events are collected using the hadronic razor trigger, we require baseline cuts of $M_R > 500\,\text{GeV}$ and $R^2 > 0.25$, in order to reach the plateau region of the trigger turn-on curve. The razor trigger efficiency in the plateau region was evaluated using a dedicated trigger, and is found to be 97%. For the Electron Multijet and Muon Multijet event categories, the baseline cuts are $M_R > 400\,\text{GeV}$ and $R^2 > 0.15$. The trigger efficiencies for electron and muon triggers are above 80% at 20 GeV, and reach a plateau above 97% around 40 GeV.

For all categories we select events that have at least four jets with $p_T > 40\,\text{GeV}$ within $|\eta| < 3.0$. In the Multijet category we also require that there are at least two jets with $p_T > 80\,\text{GeV}$ within $|\eta| < 3.0$, driven by the requirements of the hadronic razor triggers. In order to suppress the QCD multijet background in the Multijet category, we require that all events pass the $\Delta\phi < 2.8$ requirement, where $\Delta\phi$ is the azimuthal angle between the two razor hemispheres. In the Electron Multijet category we require that electrons have $p_T > 25\,\text{GeV}$, and in the Muon Multijet category, muons must have $p_T > 20\,\text{GeV}$. In order to reduce backgrounds from W+jets and $t\bar{t}$ processes in the Muon and Electron Multijet categories, events are required to pass a selection on $M_T > 120\,\text{GeV}$ (where M_T is the transverse mass of the lepton and E_T^{miss}). Events with possible contributions from beam halo processes, or anomalous noise in the calorimeter are rejected using dedicated algorithms [13].

Within each of the categories listed above, we consider separately the events which have no b-tagged jet, one b-tagged jet, two b-tagged jets, and at least three b-tagged jets. In events with zero and one b-tagged jet in the Multijet category $10-15\%$ originate from QCD multijet production, $40-60\%$ from $Z(\to \nu\nu)$+jets and $W(\to \ell\nu)$+jets, and the remaining background is dominated by $t\bar{t}$ events. Around $70-75\%$ of events with higher b-tag multiplicities in the Multijet category are from $t\bar{t}$ production. In the Electron and Muon Multijet categories, events with zero b-tagged jets are composed of $\sim 30\%$ $W \to \ell\nu$+jet and $\sim 40\%$ $t\bar{t}$, while in events with higher b-tag multiplicities $80-90\%$ are $t\bar{t}$ events.

In Table 1 we summarize the event selection criteria required for each event category considered in this analysis. Events that fall into these categories form the search regions used in this analysis.

3.2 Simplified SUSY models

In this analysis, three simplified models [14–19] are considered for gluino pair production, based on three-body gluino decays [20]. The lightest supersymmetric particle (LSP) is the lightest neutralino $\tilde{\chi}_1^0$. All other SUSY particles are assumed to be too heavy to participate in the

Table 1: Summary of the selection criteria and b-tag bins used to define the analysis search regions.

Event category	B-Tag bins	Selection cuts
Electron + Multijet	0 b-tag, 1 b-tag, 2 b-tag, 3 or more b-tags	single electron triggered events, one tight electron, $p_T(e) > 25$ GeV, $M_T > 120$ GeV, $\geq$4 jets with $p_T > 40$ GeV, $M_R > 400$ GeV, $R^2 > 0.15$
Muon + Multijet	0 b-tag, 1 b-tag, 2 b-tag, 3 or more b-tags	single muon triggered events, one tight muon, $p_T(\mu) > 20$ GeV, $M_T > 120$ GeV, $\geq$4 jets with $p_T > 40$ GeV, $M_R > 400$ GeV, $R^2 > 0.15$
Multijet	0 b-tag, 1 b-tag, 2 b-tag, 3 or more b-tags	hadronic razor triggered events, $\Delta\phi < 2.8$, no veto electrons or muons, $\geq$4 jets with $p_T > 40$ GeV, $\geq$2 jets with $p_T > 80$ GeV, $M_R > 500$ GeV, $R^2 > 0.25$

interactions. The three models considered are:

- gluino pair-production, decaying with a 100% branching fraction to a bottom quark-antiquark ($b\bar{b}$) pair and the LSP;
- gluino pair-production, decaying with a 100% branching fraction to a top quark-antiquark ($t\bar{t}$) pair and the LSP.
- gluino pair-production, decaying with a 100% branching fraction to a first or second generation quark-antiquark ($q\bar{q}$) pair and the LSP.

The corresponding pseudo-Feynman diagrams are shown in Figure 1.

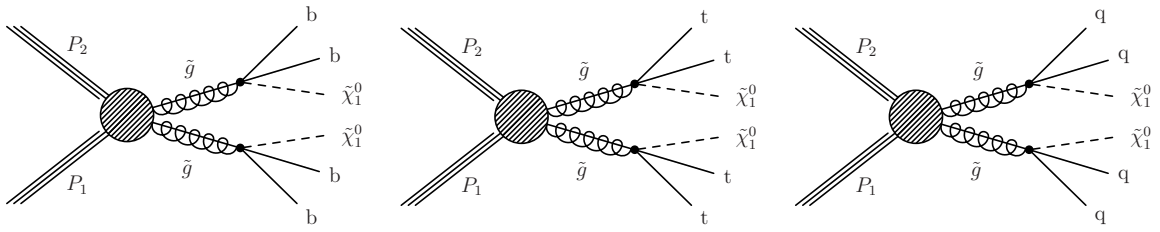

Figure 1: Diagrams displaying the event topologies of gluino pair production considered in this analysis.

Standard Model background processes and the three simplified models are generated with MADGRAPH V5 [21] interfaced with PYTHIA V8.1 [22]. Standard model processes are simulated using a Geant4-based model [23] of the CMS detector. The simulation of new physics signals is performed using the CMS fast simulation package [24]. Simulated events are processed with the same chain of reconstruction programs as used for collision data. Simulation events are reweighted according to the distribution of pileup calculated based on the measured instantaneous luminosity.

4 Background estimation

After applying the event selection requirements listed above, in each event category, we search for SUSY signal events in the two-dimensional plane of razor variables M_R and R^2. Background estimation is done using an extended, binned, maximum-likelihood fit to the M_R and R^2 distribution in two ways:

- A fit to the data in the sideband region in M_R and R^2 as a model-independent way to look for excesses or discrepancies. The fit is performed using only the data in the sideband, and the functional form is extrapolated to the full M_R and R^2 plane.
- A fit to the data in the full search region in M_R and R^2 under a background-only and a signal-plus-background hypothesis, following a modified frequentist approach (LHC CL_s) [25–28] to interpret the data in the context of particular SUSY simplified models.

The sideband region is defined to be 100 GeV in width in the M_R dimension and 0.05 in width in the R^2 dimension. Explicitly, for the Multijet event category, it comprises the region 500 GeV $< M_R <$ 600 GeV and $R^2 > 0.3$, plus the region $M_R >$ 500 GeV and $0.25 < R^2 < 0.3$. For the Muon Multijet and Electron Multijet event categories, it comprises the region 400 GeV $< M_R <$ 500 GeV and $R^2 > 0.2$, plus the region $M_R >$ 400 GeV and $0.15 < R^2 < 0.2$. The rectangular region within the search region but outside of the sideband region is referred to as the "signal-sensitive region." The definitions of the sideband and signal-sensitive regions, and the corresponding bins, are summarized in Figure 2.

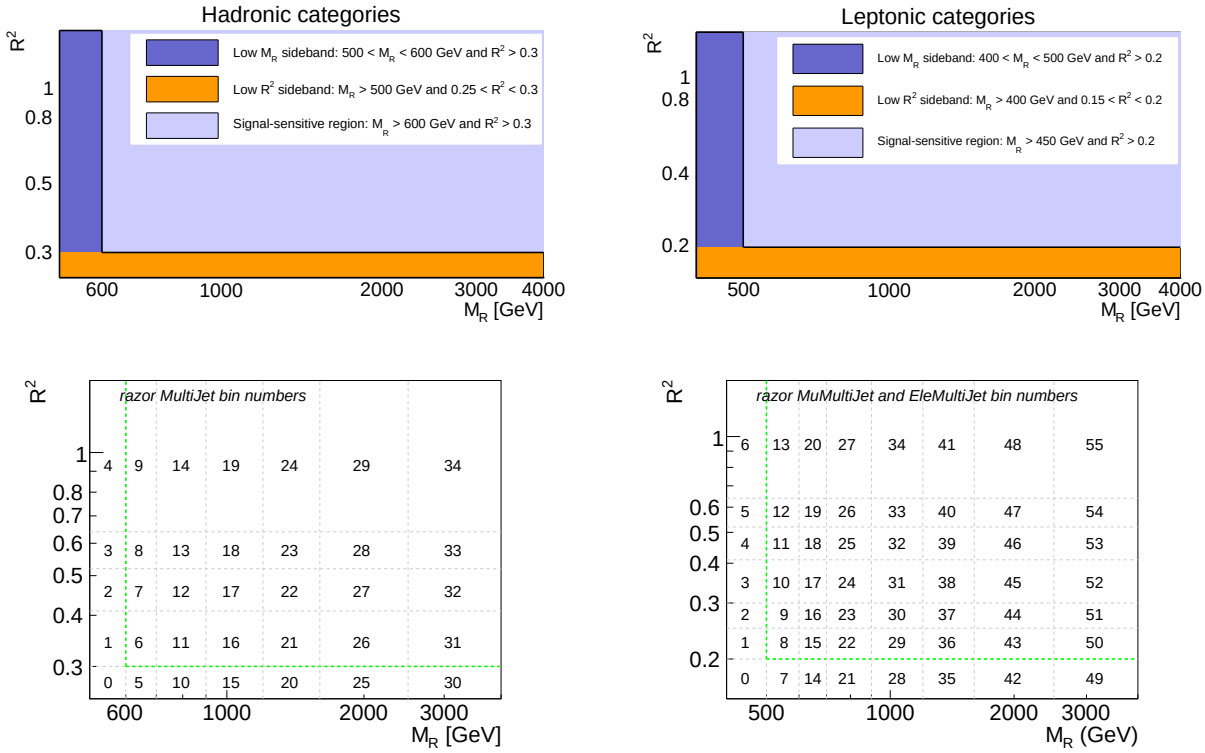

Figure 2: Definition of the sideband and the signal-sensitive regions used in the analysis, for (top left) the zero lepton category and (top right) the one lepton categories. Definition of the bin numbers associated to each region in the R^2-M_R plane for (bottom left) the zero lepton category and (bottom right) the one lepton categories.

Based on the analysis of CMS Run 1 data collected at 7 and 8 TeV, and studies of simulated backgrounds at 13 TeV, the two-dimensional probability density function for the SM background processes is found to be well described by the empirical function of the following form:

$$f_{\mathrm{SM}}(M_R, R^2) = \left[b(M_R - M_R^0)^{1/n}(R^2 - R_0^2)^{1/n} - 1\right] e^{-bn(M_R - M_R^0)^{1/n}(R^2 - R_0^2)^{1/n}}. \quad (5)$$

The shape is described by four parameters: M_R^0, R_0^2, b, and n. The last two parameters, b and n, determine the tail of the distribution on the two-dimensional plane, while the M_R^0 (R_0^2) parameter affects the tail of the one-dimensional projection on R^2 (M_R). For $n = 1$, the function projects to an exponential both on R^2 and M_R, and b is proportional to the exponential rate parameter in each one-dimensional projection.

For each event category, we fit the two-dimensional distribution of M_R and R^2 in the sideband region using the above functional form, separately for events with no b-tagged jets, one b-tagged jet, two b-tagged jets, and three or more b-tagged jets. The normalization in each event category and each b-tagged jet bin is floated in the fit independently and unconstrained. Due to the lack of data events in the category with three or more b-tagged jets, we constrain the shape of this category to be related to the shape for events with two b-tagged jets with the following relationship:

$$f_{\mathrm{SM}}^{3\mathrm{b}}(M_R, R^2) = (1 + m_{M_R}(M_R - M_R^{\mathrm{offset}}))f_{SM}^{2b}(M_R, R^2), \quad (6)$$

where $f_{\mathrm{SM}}^{2\mathrm{b}}(M_R, R^2)$ and $f_{\mathrm{SM}}^{3\mathrm{b}}(M_R, R^2)$ are the probability density functions for events with two b-tagged jets and with three or more b-tagged jets, respectively; M_R^{offset} is the lowest M_R value in a particular event category; and m_{M_R} is a floating parameter constrained by a Gaussian distribution centered at the value measured using Monte Carlo simulation and with a 100% uncertainty. The above form for the shape of the background events with three or more b-tagged jets was verified in Monte Carlo simulation.

Numerous tests were performed to establish the robustness of the fit model in adequately describing the underlying distributions. To demonstrate that the background model gives an accurate description of the background distributions, we construct a representative dataset using MC simulated samples, and perform the background fit using the functional form from Eq. 5. Goodness-of-fit is evaluated by comparing the background prediction from the fit with the prediction from the MC simulation. This procedure is performed separately for each of the search categories. These comparisons demonstrate that the fit function yields an accurate representation of the background predicted by the Monte Carlo simulation. Tests done for datasets that are about ten times larger than the LHC 2015 dataset collected by CMS yielded goodness-of-fit "p"-values over the M_R and R^2 plane ranging from 40% to 3%.

We also demonstrate that the fit model is robust against variations of the background composition predicted by the Monte Carlo simulations by altering relative contributions of the major backgrounds by a large amount and performing a new fit on this alternative background composition. We then compare the results of this fit to the nominal fit prediction. For the Multijet event category the dominant backgrounds are $\mathrm{t\bar{t}}$, W+jets, and $\mathrm{Z} \to \nu\nu$. We vary the contribution of each process up and down by 30% and perform fits in each configuration. One of the potentially difficult backgrounds to model is QCD multijet production, which has significant contribution in the Multijet category. We observe in the Monte Carlo simulation that the shapes of the QCD multijet process are not significantly different from the mixture of all other backgrounds. Furthermore, we extend the robustness tests by varying the contribution of the QCD multijet process up by 50% and 100%. In order to verify that our fit robustness tests incorporate a reliable QCD simulation, we perform a check in a QCD enriched sample of events that are

selected by requiring 2 or 3 jets and $\Delta\phi > 2.8$. This data sample is composed of $\sim 80\%$ QCD production, with the rest dominated by W+jets, and $Z \to \nu\nu$. We find that the QCD simulation describes the data in this control sample well, with proper modeling of the shapes of the M_R and R^2 distributions.

For the Muon Multijet and Electron Multijet event categories, the main background is $t\bar{t}$. However the event kinematics are slightly different depending on whether both top quarks decayed leptonically, or whether only one of the top quarks decayed leptonically. About $75\% - 85\%$ of the $t\bar{t}$ background in the search region are events where both top quarks decayed leptonically. We test the robustness of the fit model to the composition of one-lepton and two-lepton decays of the top quark pairs by increasing and decreasing each component by 30%. We also test for the robustness of the fit model against errors in the Monte Carlo prediction for the rare backgrounds, such as $t\bar{t}Z$, which makes up a significant fraction of the background at large values of M_R. The contribution from these rare backgrounds are increased by 100% and decreased by 50%, and fits with the same function are performed. In each of these tests, we show that the chosen functional form can adequately describe the shapes of the M_R and R^2 distributions as predicted by the Monte Carlo simulation.

For the sideband analysis, the background shape parameters are estimated from the events in the sideband region. The fitted shape is then used to derive a background prediction in the signal-sensitive region. To quantify the agreement between the background model and the observation, we generate alternative sets of background shape parameters from the covariance matrix returned by the fit. An ensemble of pseudo-experiment data sets is created, generating random (M_R, R^2) pairs distributed according to each of these alternative shapes. For each bin of the signal-sensitive region, the distribution of the predicted yields in each pseudo-experiment is compared to the observed yield in data in order to quantify the agreement between the background model and the observation.

To demonstrate that (1) the model-independent sideband fit procedure used in the analysis would be able to indicate the presence of a signal and that (2) the model-dependent full fit procedure used in the analysis would be able to extract the signal strength in an unbiased way, we perform two separate signal injection tests.

For the former, we sample a signal-plus-background toy dataset and perform a background-only fit in the sideband. As an illustrative example, we show one example of such a test in Figure 3 where we inject a signal corresponding to gluino pair production, in which each gluino decays to a neutralino and a $b\bar{b}$ pair with $m_{\tilde{g}} = 1400\,\text{GeV}$ and $m_{\tilde{\chi}} = 100\,\text{GeV}$. The deviations with respect to the fit predictions are shown for the 2 b-tag and ≥ 3 b-tag categories. We observe characteristic patterns of excesses in two adjacent strips in the M_R dimension. For signal models in the compressed region of model parameter space, which have smaller mass splitting between the gluino and the lightest neutralino, a different pattern of excess appears, where bins at large values of R^2 are more evenly populated. In general, signals with smaller mass splitting exhibit less of a peak in M_R and more of a longer tail, and will therefore contaminate the sideband region. Therefore it is generally much more difficult and requires larger datasets to interpret such a situation as a discovery.

To demonstrate that the model-specific full fit procedure is able to extract the signal strength in an unbiased way, test an ensemble of signal-plus-background toy experiments and demonstrate that we can accurately measure the injected signal strength. We perform the signal injection using gluino pair-production simplified models signals, where gluinos decay with a 100% branching fraction to a $b\bar{b}$ pair and the LSP. Using the background model obtained from the best fit to the Monte Carlo simulation of the backgrounds, we randomly draw a number

of events corresponding to the expected background yield. In addition we randomly draw a number of signal events from a template histogram built from the Monte Carlo simulation of the signal, and combine it with the background events to form a pseudo-experiment. An ensemble of pseudo-experiments is obtained by repeating this procedure multiple times. For each pseudo-experiment, a fit to the signal plus background model is performed, and the number of signal events is extracted. Finally, we compare the average signal size over the entire ensemble of pseudo-experiments to the input signal size to evaluate the accuracy of the signal extraction procedure. Signal models with high mass splitting ($m_{\tilde{g}} = 1500\,\text{GeV}$ and $m_{\tilde{\chi}} = 100\,\text{GeV}$) and signal models in the compressed region ($m_{\tilde{g}} = 1000\,\text{GeV}$ and $m_{\tilde{\chi}} = 900\,\text{GeV}$) were tested and in both cases we observe that the fit procedure is able to extract the correct signal strength with no bias.

Additional studies were performed comparing the background prediction from the sideband fit and the full region fit to evaluate the average deviation of the two fit predictions. The best fit background shape is used as a probability density function and sampled to obtain an ensemble of toy experiments. For each toy experiment, we perform a sideband fit and a full region fit, and the fit predictions for the background yield in the region at high M_R and high R^2 are compared on a toy-by-toy basis. For the zero lepton category, the region is defined as $M_R > 700\,\text{GeV}$ and $R^2 > 0.41$, while for the one lepton categories, the region is defined as $M_R > 500\,\text{GeV}$ and $R^2 > 0.25$. We observe that on average the sideband fit predicts a slightly smaller background yield in these regions compared to the full region fit, and that the average difference decreases with increasing integrated luminosity. For the zero lepton category the average difference decreases from about 15% for data samples corresponding to $2\,\text{fb}^{-1}$ to less than 2% for data samples corresponding to about $20\,\text{fb}^{-1}$, while for the one lepton categories the average difference decreases from about 15% to about 7%. The difference is small compared to the total systematic uncertainty, which ranges from 40% to 100% depending on the b-tag bin. We propagate an extra systematic uncertainty into the background prediction, to cover these average differences between the sideband fit and the full region fit.

Since the background prediction in this analysis is entirely data-driven, the uncertainties on the background prediction are propagated through the binned maximum-likelihood fit procedure. For more populated bins such as the 0 b-tag and 1 b-tag bins in the MultiJet category, the systematic uncertainties range from about 30% at low M_R and R^2 to about 70% at high M_R and R^2. For sparsely populated bins such as the 3 or more b-tag bin in the Muon MultiJet or Electron MultiJet categories, the systematic uncertainties range from about 60% at low M_R and R^2 to more than 200% at high M_R and R^2.

5 Signal models and the systematic uncertainties

We propagate systematic uncertainties on the signal due to instrumental and theoretical effects as a shape uncertainty on the signal prediction in the different event categories. These uncertainties affect both the shape of the M_R and R^2 distributions as well as the signal efficiency. The systematic uncertainties include the uncertainties on the lepton selection efficiency, lepton trigger efficiency, b-tagging efficiency, jet energy scale, integrated luminosity, pileup, missing higher order corrections, and parton distribution functions. In Table 2, we list the approximate size of these systematic uncertainties.

Table 2: Effect of systematic uncertainties on the expected signal yields. The range of systematic uncertainties quoted vary with $m_{\tilde{g}}$ and $m_{\tilde{\chi}}$ parameters of specific signal models.

Systematic Uncertainty Source	Uncertainty
Lepton Selection Efficiency	2%
Fast Simulation Lepton Selection Efficiency	$0-10\%$
Lepton Trigger Efficiency	3%
B-Tagging Efficiency	$5-15\%$
Fast Simulation B-Tagging Efficiency	$0-10\%$
Jet Energy Scale	$5-10\%$
Luminosity	4.6%
Ren./Fac. Scale	$3-5\%$
Parton Distribution Functions	10%
Initial State Radiation	$2\%-20\%$
Pileup	$<1\%$
Monte Carlo Statistics	$0-10\%$

6 Results

In this section we present the results of the search for SUSY signal events performed in the search regions described in this note. The number of events observed in data are compared to the prediction from the sideband fit in the M_R and R^2 bins described in Section 4 in Figures 4, 5 and 6 for the MultiJet, Muon Multijet, and Electron Multijet event categories respectively. The agreement between the predicted and the observed yields is described as a two-sided "p"-value and then translated into the corresponding number of standard deviations for a normal distribution. The number of standard deviations are shown in the lower part of Figures 4, 5 and 6. Positive (negative) significance indicates the observed yield is larger (smaller) than the predicted one in a particular region. We observe no statistically significant deviations from the expected background predictions.

As can be seen from Figures 4-6, we do not observe any significant excess in data, hence we set upper limits on the production cross section for specific simplified models motivated by SUSY. For each given signal model, we use the asymptotic approximation of the LHC-type CL_s limit setting prescription, by performing maximum-likelihood fits under both the signal plus background hypothesis and the background only hypothesis and comparing appropriate likelihood ratios. Systematic uncertainties are propagated through the inclusion of additional nuisance parameters that induce both shape and normalization variations on the signal and background predictions. Results are interpreted as 95% confidence level (CL) upper limits on the production cross section for simplified models introduced in section 3.2, and are shown in Figures 7, 8, and 9 for the gluino pair-production simplified models signals, where gluinos decay with a 100% branching fraction to an LSP and a $b\bar{b}$, $t\bar{t}$, or $q\bar{q}$ pair respectively. Assuming the lightest supersymmetric particle has a mass of 100 GeV, the pair production of gluinos in multi-bottom-quark and multi-top-quark final states is excluded for gluino masses up to 1650 GeV and 1600 GeV, respectively. For the case of final states with first or second generation quarks, gluinos up to 1350 GeV in mass are excluded. In Figure 10 we show a comparison of the observed and expected exclusion limits on various simplified models.

7 Summary

We presented the results of a search for SUSY production using razor variables at $\sqrt{s} = 13$ TeV, using 2.1 fb^{-1} data collected by CMS experiment at the LHC in 2015. In the absence of significant deviations from the predicted background we set limits on the production cross section of specific signal models. For a neutralino lightest supersymmetric particle of mass 100 GeV, the pair production of gluinos is excluded at 95% CL for gluino masses up to 1650 GeV, assuming the gluino decays to a neutralino and a bottom quark-antiquark pair. For the corresponding decays to top quarks and first or second generation quarks, gluinos with masses up to 1600 GeV and 1350 GeV are excluded, respectively.

References

[1] C. Rogan, "Kinematics for new dynamics at the LHC", (2010). arXiv:1006.2727.

[2] CMS Collaboration, "Inclusive search for squarks and gluinos in pp collisions at $\sqrt{s} = 7$ TeV", *Phys. Rev. D* **85** (2012) 012004, doi:10.1103/PhysRevD.85.012004, arXiv:1107.1279.

[3] CMS Collaboration, "Inclusive search for supersymmetry using the razor variables in pp collisions at $\sqrt{s} = 7$ TeV", *Phys. Rev. Lett.* **111** (2013) 081802, doi:10.1103/PhysRevLett.111.081802, arXiv:1212.6961.

[4] CMS Collaboration, "Search for supersymmetry with razor variables in pp collisions at $\sqrt{s} = 7$TeV", *Phys. Rev. D* **90** (2014), no. 11, 112001, doi:10.1103/PhysRevD.90.112001, arXiv:1405.3961.

[5] CMS Collaboration, "Search for Supersymmetry Using Razor Variables in Events with b-Tagged Jets in pp Collisions at $\sqrt{s} = 8$ TeV", *Phys. Rev.* **D91** (2015) 052018, doi:10.1103/PhysRevD.91.052018, arXiv:1502.00300.

[6] ATLAS Collaboration, "Multi-channel search for squarks and gluinos in $\sqrt{s} = 7$ TeV pp collisions with the ATLAS detector", *Eur. Phys. J. C* **73** (2013) 2362, doi:10.1140/epjc/s10052-013-2362-5, arXiv:1212.6149.

[7] ATLAS Collaboration, "Search for squarks and gluinos in events with isolated leptons, jets and missing transverse momentum at $\sqrt{s} = 8TeV$ with the ATLAS detector", *JHEP* **116** (2015), no. 4, doi:10.1007/JHEP04(2015)116.

[8] CMS Collaboration, "Particle-flow event reconstruction in CMS and performance for jets, taus, and $E_{\mathrm{T}}^{\mathrm{miss}}$", CMS Physics Analysis Summary CMS-PAS-PFT-09-001, 2009.

[9] CMS Collaboration, "Commissioning of the particle-flow event with the first LHC collisions recorded in the CMS detector", CMS Physics Analysis Summary CMS-PAS-PFT-10-001, 2010.

[10] M. Cacciari, G. P. Salam, and G. Soyez, "The anti-k_t jet clustering algorithm", *JHEP* **04** (2008) 063, doi:10.1088/1126-6708/2008/04/063, arXiv:0802.1189.

[11] M. Cacciari, G. P. Salam, and G. Soyez, "FastJet user manual", *Eur. Phys. J. C* **72** (2012) 1896, doi:10.1140/epjc/s10052-012-1896-2, arXiv:1111.6097.

[12] CMS Collaboration, "Performance of b-Tagging Algorithms in 50ns Data at 13 TeV", Technical Report CMS-DP-2015-045, Sep, 2015.

[13] CMS Collaboration, "Missing transverse energy performance of the CMS detector", *Journal of Instrumentation* **6** (2011), no. 09, P09001.

[14] N. Arkani-Hamed et al., "MARMOSET: The Path from LHC Data to the New Standard Model via On-Shell Effective Theories", (2007). arXiv:hep-ph/0703088.

[15] J. Alwall, P. C. Schuster, and N. Toro, "Simplified models for a first characterization of new physics at the LHC", *Phys. Rev. D* **79** (2009) 075020, doi:10.1103/PhysRevD.79.075020, arXiv:0810.3921.

[16] J. Alwall, M.-P. Le, M. Lisanti, and J. G. Wacker, "Model independent jets plus missing energy searches", *Phys. Rev. D* **79** (2009) 015005, doi:10.1103/PhysRevD.79.015005, arXiv:0809.3264.

[17] D. S. M. Alves, E. Izaguirre, and J. G. Wacker, "Where the sidewalk ends: jets and missing energy search strategies for the 7 TeV LHC", *JHEP* **10** (2011) 012, doi:10.1007/JHEP10(2011)012, arXiv:1102.5338.

[18] LHC New Physics Working Group Collaboration, "Simplified models for LHC new physics searches", *J. Phys. G* **39** (2012) 105005, doi:10.1088/0954-3899/39/10/105005, arXiv:1105.2838.

[19] M. L. Graesser and J. Shelton, "Hunting Mixed Top Squark Decays", *Phys. Rev. Lett.* **111** (2013) 121802, doi:10.1103/PhysRevLett.111.121802, arXiv:1212.4495.

[20] CMS Collaboration, "Interpretation of Searches for Supersymmetry with Simplified Models", *Phys. Rev. D* **88** (2013) 052017, doi:10.1103/PhysRevD.88.052017, arXiv:1301.2175.

[21] J. Alwall et al., "MadGraph 5: going beyond", *Journal of High Energy Physics* **2011** (2011), no. 6, doi:10.1007/JHEP06(2011)128.

[22] T. Sjöstrand, S. Mrenna, and P. Skands, "A brief introduction to PYTHIA 8.1", *Computer Physics Communications* **178** (2008), no. 11, 852 – 867, doi:http://dx.doi.org/10.1016/j.cpc.2008.01.036.

[23] S. Agostinelli et al., "Geant4 - a simulation toolkit", *Nucl. Instrum. Meth. A* **506** (2003), no. 3, 250 – 303, doi:http://dx.doi.org/10.1016/S0168-9002(03)01368-8.

[24] S. Abdullin et al., "The Fast Simulation of the CMS Detector at LHC", *Journal of Physics: Conference Series* **331** (2011), no. 3, 032049.

[25] A. L. Read, "Presentation of search results: The CL_s technique", *J. Phys. G* **28** (2002) 2693, doi:10.1088/0954-3899/28/10/313.

[26] A. L. Read, "Modified frequentist analysis of search results (The CL_s method)", *CERN-OPEN* **205** (2000).

[27] G. Cowan, K. Cranmer, E. Gross, and O. Vitells, "Asymptotic formulae for likelihood-based tests of new physics", *Eur. Phys. J. C* **71** (2011) 1554, doi:10.1140/epjc/s10052-011-1554-0, arXiv:1007.1727.

[28] ATLAS and CMS Collaborations, "Procedure for the LHC Higgs boson search combination in summer 2011", CMS NOTE/ATL-PHYS-PUB ATL-PHYS-PUB-2011-011, CMS-NOTE-2011-005, 2011.

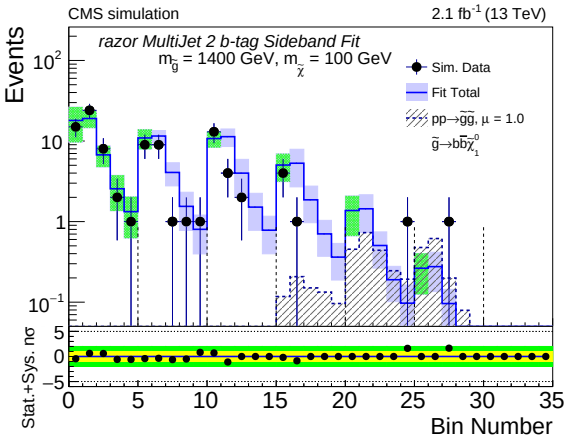

(a) 2 b-tag

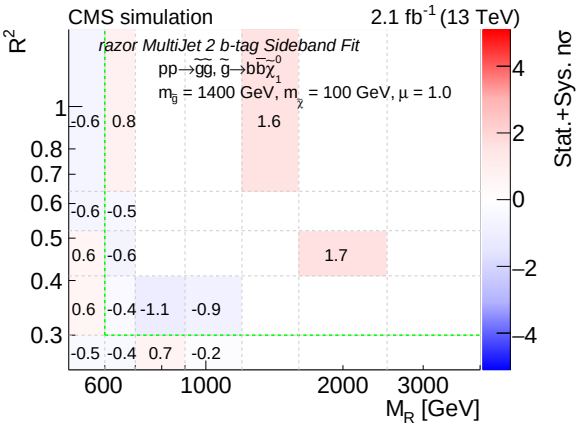

(b) 2 b-tag

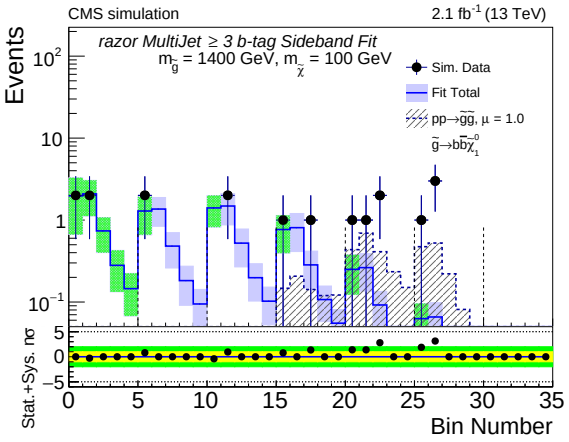

(c) ≥ 3 b-tag

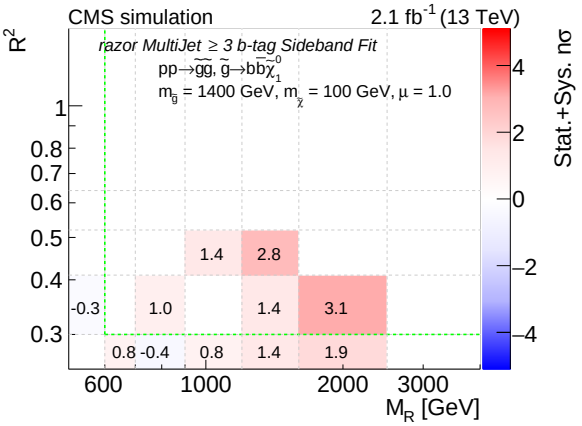

(d) ≥ 3 b-tag

Figure 3: The result of the background-only fit performed in the sideband on a signal-plus-background toy dataset using gluino pair-production simplified models signals, where gluinos decay with a 100% branching fraction to a $b\bar{b}$ pair and the LSP, with $m_{\tilde{g}} = 1400\,\text{GeV}$ and $m_{\tilde{\chi}} = 100\,\text{GeV}$, at nominal signal strength. One-dimensional representations of the fit result for the 2 b-tag (top left) and ≥ 3 b-tag categories (bottom left) are shown on the left, where the uncertainty band for the sideband bins are shown in green. Vertical dashed lines denote the boundaries of different M_R bins, as defined in Fig. 2. The distributions of deviations in the R^2-M_R plane, expressed in units of standard deviations, are shown on the right for the 2 b-tag (top right) and ≥ 3 b-tag categories (bottom right). Statistical and systematic uncertainties are both considered in the calculation of the deviations.

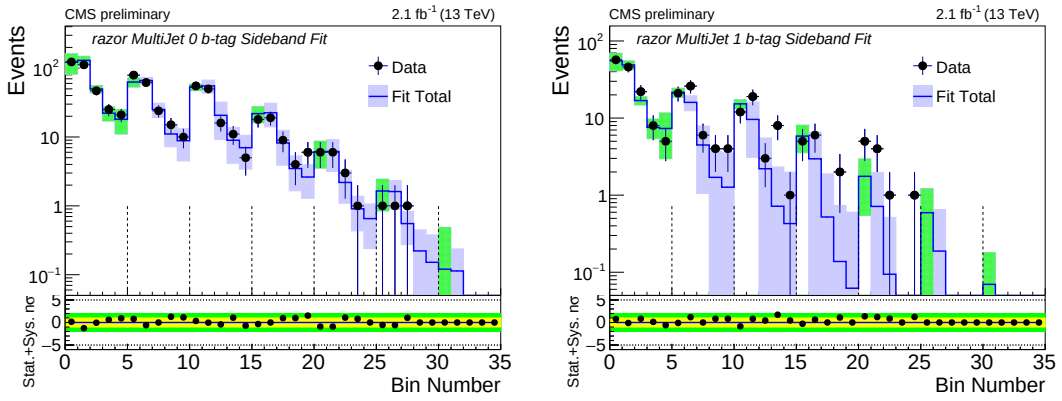

(a) 0 b-tag

(b) 1 b-tag

(c) 2 b-tag

(d) $\geq$ 3 b-tag

Figure 4: Comparison of the predicted background with the observed data in bins of M_R and R^2 variables in the Multijet category. The colored bands represents the systematic uncertainties in the background prediction. The uncertainty bands for the sideband bins are shown in green. On the bottom inset, the deviation between the observed data and the background prediction are plotted in units of standard deviation, taking into account both statistical and systematic uncertainties. Vertical dashed lines denote the boundaries of different M_R bins, as defined in Figure 2.

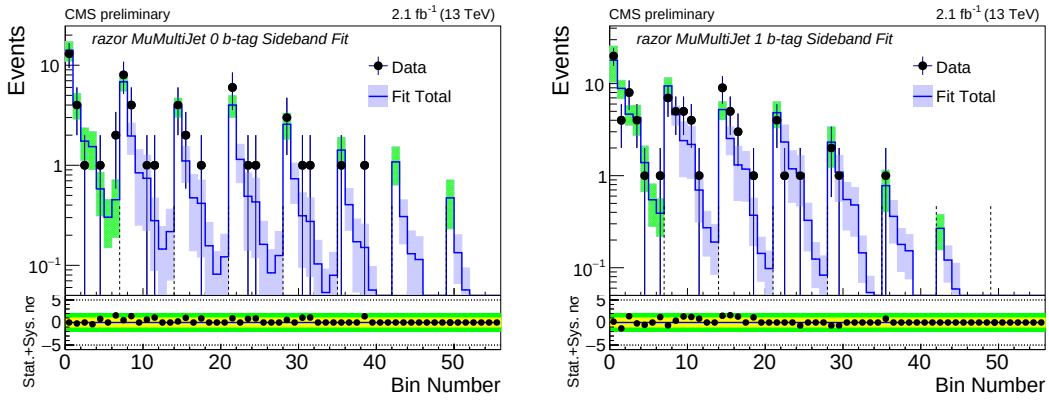

(a) 0 b-tag

(b) 1 b-tag

(c) 2 b-tag

(d) $\geq$ 3 b-tag

Figure 5: Comparison of the predicted background with the observed data in bins of M_R and R^2 variables in the Muon Multijet category. The colored bands represents the systematic uncertainties in the background prediction. The uncertainty bands for the sideband bins are shown in green. On the bottom inset, the deviation between the observed data and the background prediction are plotted in units of standard deviation, taking into account both statistical and systematic uncertainties. Vertical dashed lines denote the boundaries of different M_R bins, as defined in Figure 2.

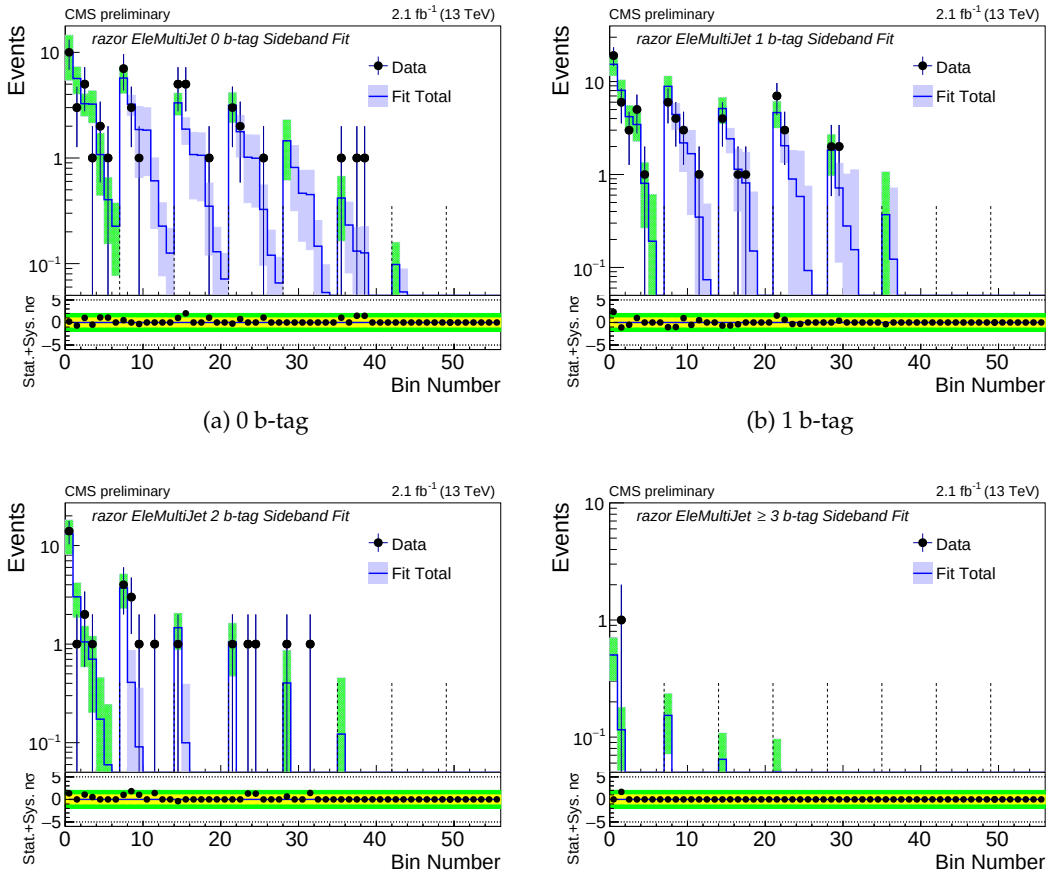

(a) 0 b-tag

(b) 1 b-tag

(c) 2 b-tag

(d) $\geq$ 3 b-tag

Figure 6: Comparison of the predicted background with the observed data in bins of M_R and R^2 variables in the Electron Multijet category. The colored bands represents the systematic uncertainties in the background prediction. The uncertainty bands for the sideband bins are shown in green. On the bottom inset, the deviation between the observed data and the background prediction are plotted in units of standard deviation, taking into account both statistical and systematic uncertainties. Vertical dashed lines denote the boundaries of different M_R bins, as defined in Figure 2.

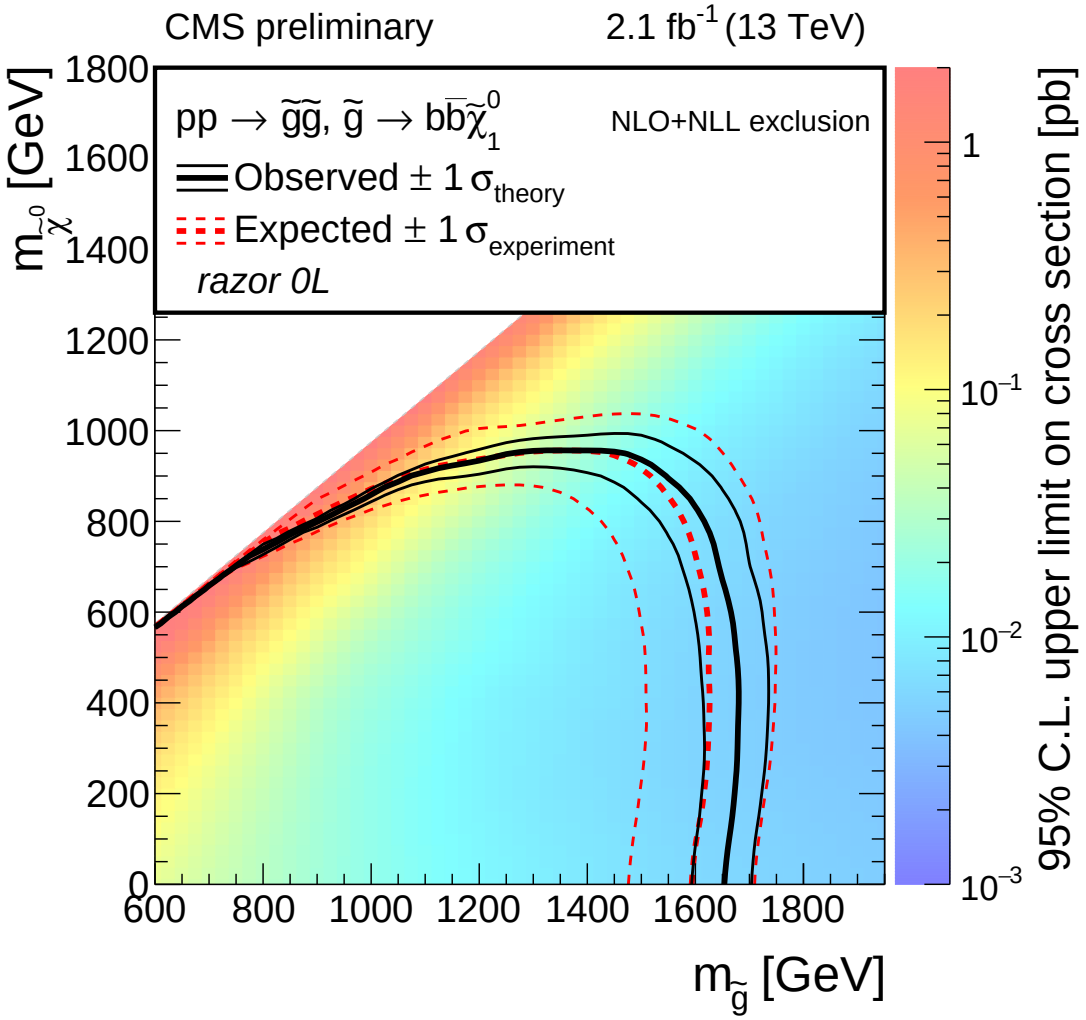

Figure 7: Interpretation of the search results with razor variables in the context of the gluino pair-production simplified model, in which the gluino decays with a 100% branching fraction to a $b\bar{b}$ pair and the LSP. The color coding indicates the observed 95% CL upper limit on the signal cross section. The dashed and solid lines represent the expected and observed exclusion contours at 95% CL, respectively. The solid contours around the observed limit and the dashed contours around the expected one represent the one standard deviation theoretical uncertainties in the cross section and the combination of the statistical and experimental systematic uncertainties, respectively.

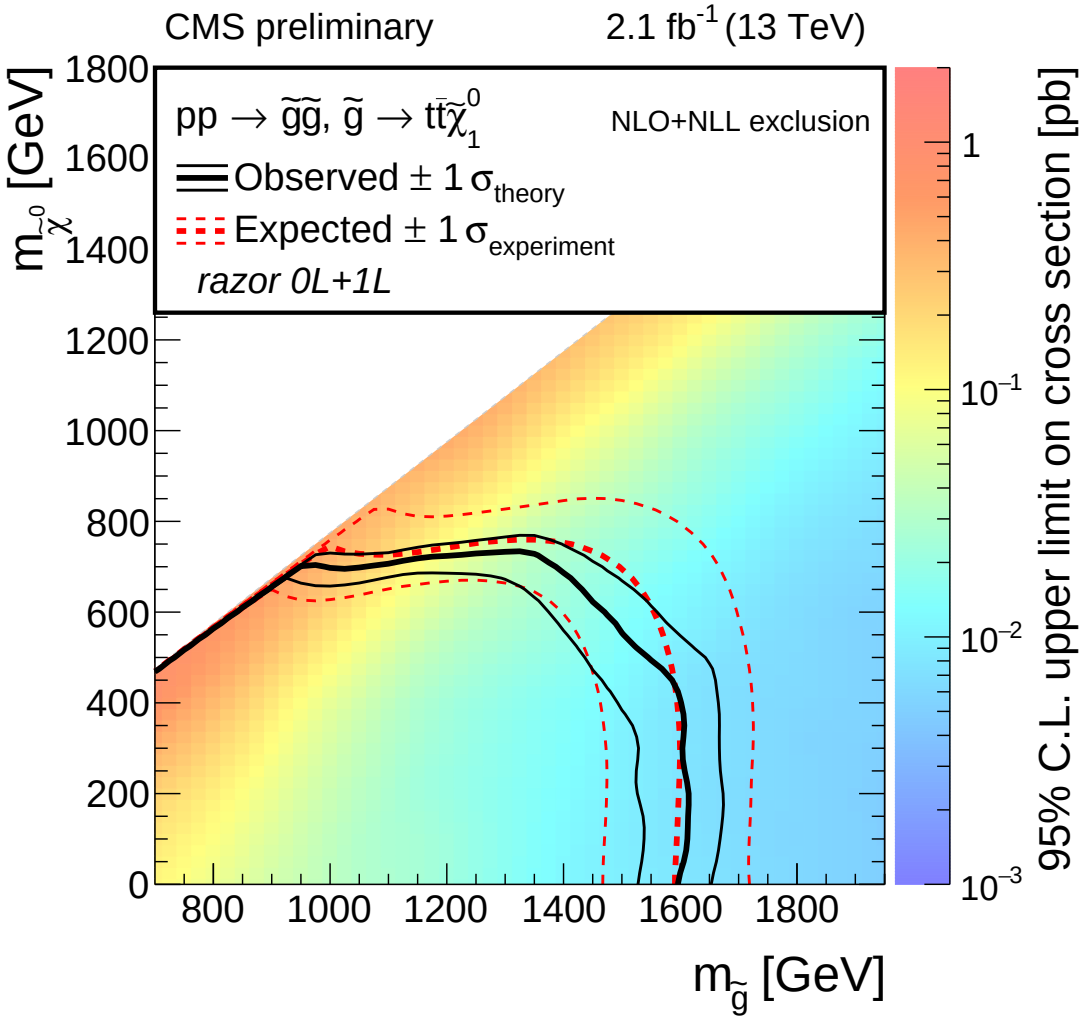

Figure 8: Interpretation of the search results with razor variables in the context of the gluino pair-production simplified model, in which the gluino decays with a 100% branching fraction to a $t\bar{t}$ pair and the LSP. The color coding indicates the observed 95% CL upper limit on the signal cross section. The dashed and solid lines represent the expected and observed exclusion contours at 95% CL, respectively. The solid contours around the observed limit and the dashed contours around the expected one represent the one standard deviation theoretical uncertainties in the cross section and the combination of the statistical and experimental systematic uncertainties, respectively.

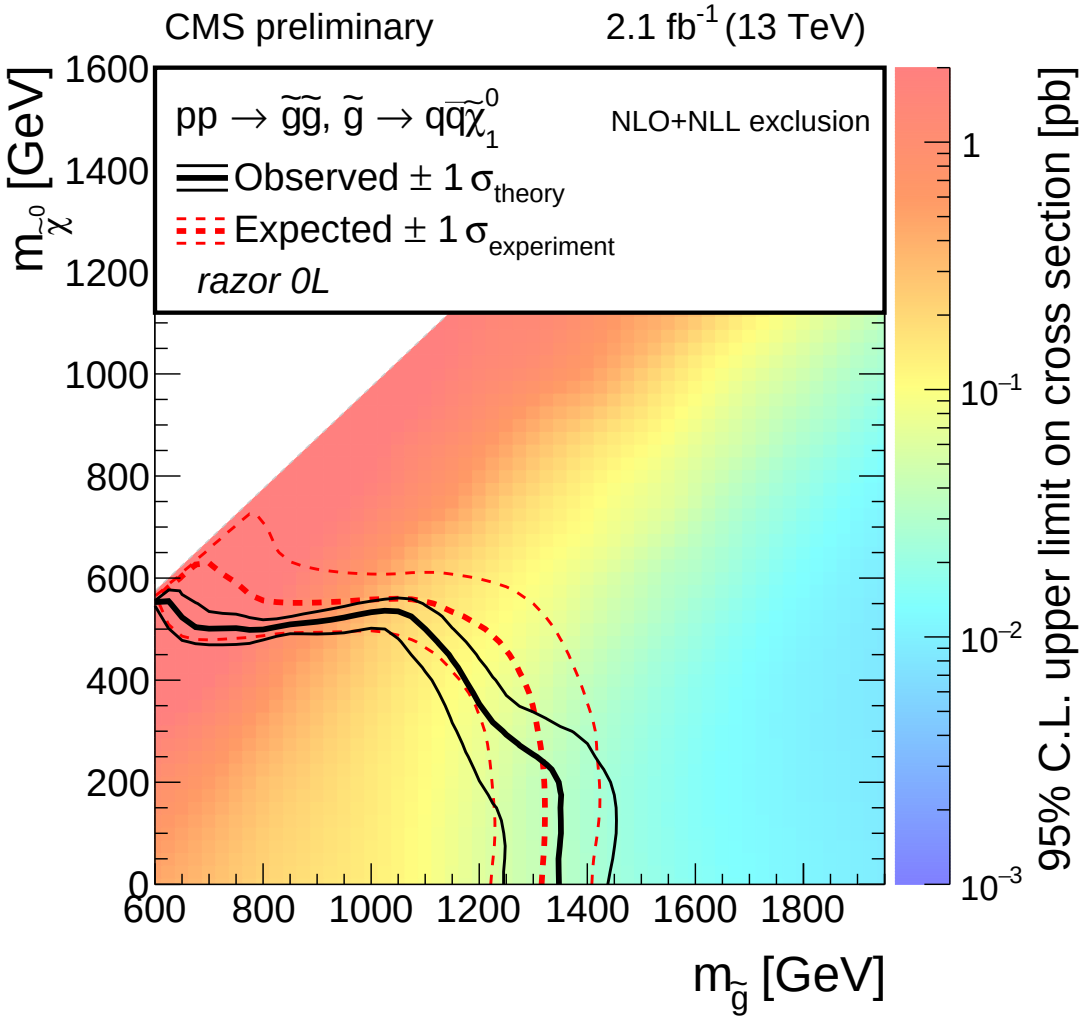

Figure 9: Interpretation of the search results with razor variables in the context of the gluino pair-production simplified model, in which the gluino decays with a 100% branching fraction to a $q\bar{q}$ pair and the LSP. The color coding indicates the observed 95% CL upper limit on the signal cross section. The dashed and solid lines represent the expected and observed exclusion contours at 95% CL, respectively. The solid contours around the observed limit and the dashed contours around the expected one represent the one standard deviation theoretical uncertainties in the cross section and the combination of the statistical and experimental systematic uncertainties, respectively.

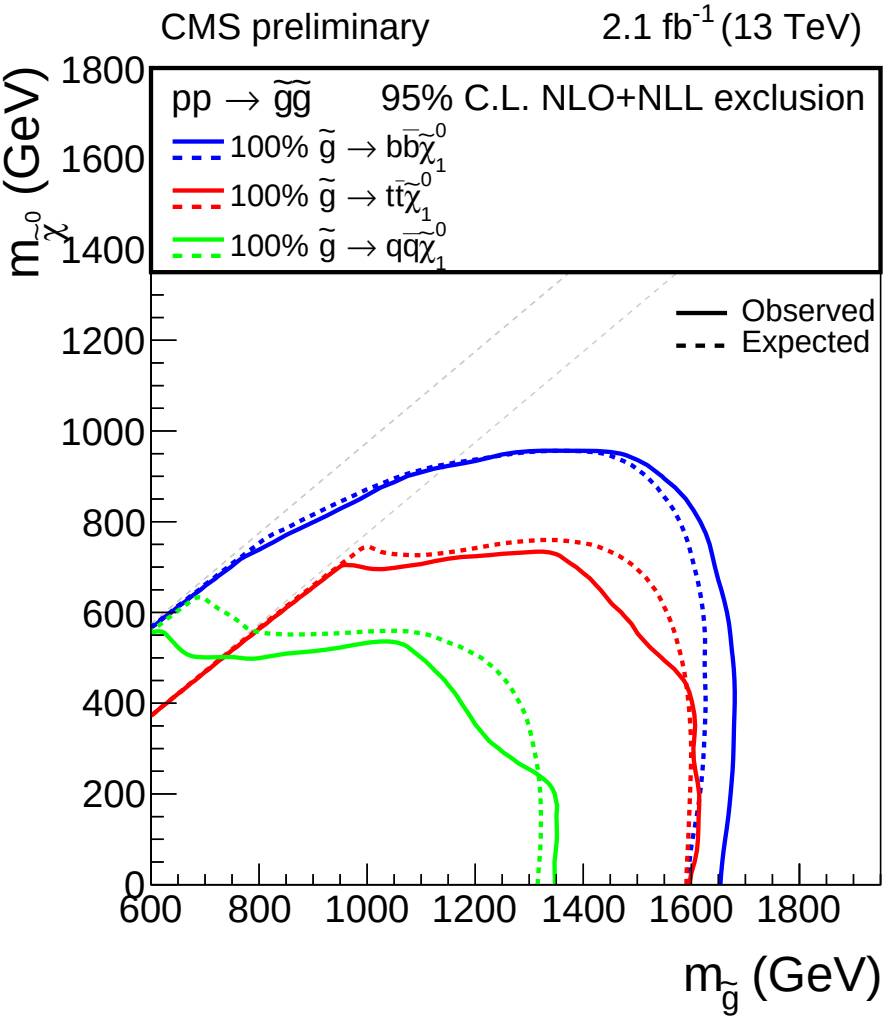

Figure 10: Summary of the exclusion contours at 95% CL in the context of gluino pair-production simplified models signals, where gluinos decay with a 100% branching fraction to an LSP and a $b\bar{b}$, $t\bar{t}$, and $q\bar{q}$ pair respectively. The dashed and solid lines represent the expected and observed exclusion contours at 95% CL, respectively. The two dashed diagonal lines indicate the boundaries of the respective mass scans ($m_{\tilde{g}} = m_{\tilde{\chi}^0} + 25$ GeV for the simplified model with bottom quarks and first or second generation quarks in the final state and $m_{\tilde{g}} = m_{\tilde{\chi}^0} + 225$ GeV for for the simplified model with top quarks in the final state).